Non-exponential temporal decay of *in vivo* MRS metabolite signals at 11.7 Tesla

D. van Ormondt, R. de Beer
Applied Physics Laboratory
TU Delft, NL

J.W.C. van der Veen
MRS Core Facility
NIMH, NIH
Bethesda, USA

D.M. Sima
ESAT-SCD
KU Leuven, BE

D. Graveron-Demilly
Creatis, Univ Lyon 1
Villeurbanne, FR

***Abstract*—MRI-scanners enable non-invasive, *in vivo* quantitation of metabolites in, *e.g.*, the brain of a patient. Among other things, this requires adequate estimation of the unknown temporal decay function of the complex-valued signal emanating from the metabolites. The first scanner for humans with a magnetic field as strong as 11.7 Tesla may become operational in the Summer of 2016. We pay attention to the possible form of the temporal decay of the signal at such a very strong field.**

***Index Terms* — metabolite quantitation, signal-decay function, 11.7 Tesla, semi-parametric estimation.**

I. Introduction

The first ever deployment of a magnet with a field as strong as B = 11.7 Tesla for whole-human (officially, 'whole-body') nuclear Magnetic Resonance Imaging (MRI) and Spectroscopy (MRS) is expected in the year 2016 [1]. The previous high-field record for whole humans was B = 9.4 Tesla [2]. The increase of B will result in increased SNR and increased spatial and spectral resolution. The latter advantages provide the main drive toward higher B. An additional consequence of higher B is that human tissue heterogenity and concomitant magnetic susceptibility effects, which are proportional to B, will become a dominant source of field inhomogeneity [2]. Inhomogeneity of B, in turn, causes acceleration of the temporal decay of the MRS signal, leading to a decrease of the potential signal-to-noise ratio (SNR), which is a disadvantage, however. At the same, increased susceptibility effects enhance detection of diseased tissue[3], which is an advantage; the latter is beyond the scope of our research.

Our goal is optimal estimation of the concentration of metabolite species contributing to an *in vivo* Magnetic Resonance Spectroscopy (MRS) signal at 11.7 Tesla. Optimality requires complete knowledge of the correct physical model function of the MRS time-domain signal, *i.e.*, including the model function of its temporal decay. Partial lack of knowledge forces us to fall back from parametric estimation to semi-parametric estmation [4]. In the present case we estimate the decay function numerically from the MRS data, in a separate procedure.

In essence, this work pertains to estimating the amplitudes of multiple metabolite signals, each with an unknown temporal decay function, from a noisy MRS-signal.

II. Methods

A. *In vivo MRS Model function for metabolites*

An *in vivo* MRS signal, here written as $s(t)$, is complex-valued. It is acquired in the time-domain [4]; t stands for time. One distinguishes contributions from metabolites and from macromolcules. The former are relatively small molecules and therefore mobile, the latter are large and hence rather restricted in their motion. The decay of metabolite signals is relatively slow, resulting in narrow features in the spectral domain. The reverse is true for macromolecules, *i.e.*, the decay of their signals is fast and the corresponding spectral shapes are broad. As already indicated in the Title, the present work focuses on the decay of metabolite signals. The *in vivo* concentrations of particular metabolite species serve as bio-markers in the diagnosis of diseases.

Ignoring noise momentarily, we model the contribution from M metabolite species $m = 1, \ldots, M$ to the signal here by [5]

$$s(t) \;=\; e^{\imath\varphi_0} \sum_{m=1}^{M} d_m(t)\; c_m\; s_m(t)\; e^{\,\imath\,(2\pi \triangle\nu_m t + \varphi_m)} \quad (1)$$

in which $d_m(t)$ is the temporal decay function of metabolite species m. Other symbols are explained further down.

It should be pointed out that in Ref. [5], the decay was assumed to be independent of m. This restriction is now dropped.

Often, the *in vivo* MRS community uses the convenient real-valued single exponential, $d_m(t) = e^{\alpha_m t}$, with $\alpha_m < 0$. The physically conjugate entity of $d_m(t)$, the line-shape $f_m(\nu)$ where ν stands for the frequency in the spectral domain, is obtained by Fourier transformation. Recall that the spectral line-shape corresponding to $e^{\alpha_m t}$ is the well-known symmetric Lorentzian function. We seek more realistic functions that account for tissue heterogeneity and susceptibility effects at high B. In general, a decay function is complex-valued.

As for other symbols in Eq. (1), $\imath^2 = -1$, φ_0 is an overall phase, $\triangle\nu_m$ and φ_m are nuisance parameters (for clinicians, that is). The quantities c_m are the amounts or concentrations of the MRS-visible metabolite species, $m = 1, \ldots, M$ to be estimated. They are the most important pieces of information for clinicians. The $s_m(t)$, $m = 1, \ldots, M$ are known, non-decaying versions of the model functions of the different metabolite species; they are computed from known molecular

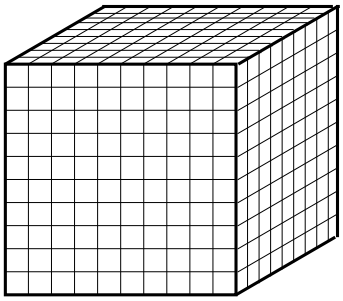

Figure 1. The volume of interest that contributes the *in vivo* MRS signal, is called voxel. Here it is fictitiously divided into many sub-voxels. The distribution of values of $B_{\rm local}(\vec{r})$ over the sub-voxels, is written as $P(B_{\rm local}(\vec{r}))$. Convolution of this function with the line-shape that would be measured in a homogeneous magnetic field yields the net line-shape in the spectral domain. See also the text below.

parameters and settings of the scanner. Fig. 1 in Ref. [5] shows the spectra of the $s_m(t)$ used in this work.

B. *Handling tissue heterogeneity effect on the model function*

As already alluded to in Sec. I, the combination of tissue heterogenity and tissue-dependent magnetic susceptibility constitutes a source of local magnetic field inhomogeneity and concomitant decay of the signal. This can be seen as follows. The net magnetic field $B_{\rm local}$ at position $\vec{r} = (x, y, z)$ of a nucleus of interest is the sum of the applied field B and contributions from magnetic susceptibility, $\chi_{\rm tissue}$, of the heterogeneous tissues surrounding this nucleus. As a result, $B_{\rm local}$ depends on the spatial coordinates $\vec{r}$ [3].

Next, consider the probability density function, $P(B_{\rm local}(\vec{r}))$, of $B_{\rm local}(\vec{r})$ in the volume of interest (voxel) in the tissue that contributes the MRS signal at hand. See Fig. 1. This function is governed by the combined effect of tissue heterogeneity and tissue susceptibility, $\chi_{\rm tissue}$. Convolving $P(B_{\rm local}(\vec{r}))$ with the line-shape that one would measure in a homogeneous magnetic field yields the net line-shape in the spectral domain. The greater the inhomogeneity, the wider the distribution, and therefore the faster the decay of the signal.

Details of tissue composition and locations of MRS-visible metabolite nuclei therein, are presently not available. As a consequence, computation from first principles of $P(B_{\rm local}(\vec{r}))$ for any metabolite species is not (yet) possible.[1] Under these circumstances, the functional form of MRS signal decay (spectral lineshape) at 11.7 T is unknown. However, a recent paper on Quantitative Susceptibility Mapping (QSM) [3] enabled us to glean at least some of the wanted information. See Fig. 2 and its caption.

The particular piece of information we use from Ref. [3] is its Fig. 5h which displays an *in vivo* map of the magnetic field difference $\Delta B_{\rm local}(\vec{r}) = B_{\rm local}(\vec{r}) - B_{\rm average}$ measured in a healthy brain at $B = 7$ Tesla [2]. In conformity with custom in the MR-community, $\Delta B_{\rm local}(\vec{r})$ is expressed in terms of the corresponding difference of the *precession*[3] *frequency of the nuclei* under investigation in the resultant local magnetic field[4]. The frequency, in turn, is converted to grey value, the range of -6 to +6 Hz corresponding to $0, 1, \ldots, 255$ on the grey scale.

The given high-resolution map of $B_{\rm local}(\vec{r})$ in a slice of a whole brain can now serve to obtain a 'real-world' example of $P(B_{\rm local}(\vec{r}))$ for an MRS-sized voxel, albeit only two-dimensional and pertains to nuclei of water molecules instead of metabolites. To this end we selected an arbitrary voxel-sized rectangle from the whole-brain map and zoomed it to a convenient size. The middle picture in Fig. 2 shows the result. Analysis of the latter grey-scale map with, *e.g.*, the Gnu Image Manipulation Program GIMP yields the corresponding probability density function, $P(B_{\rm local}(\vec{r}))$. The result of this is given in Sec. III, **Results**. For the moment, this serves as a proof of the reality of susceptibilty effects. A 3-dimensional version of $P(B_{\rm local}(\vec{r}))$ in turn can provide information about the temporal decay of an MRS signal originating from a voxel of interest. In future experiments at very high B, estimation of the decay of metabolite signals from a three dimensional MRI frequency-shift measurement in the manner just described, is foreseen. In the meantime, the decay function is to be estimated from the MRS data themselves. This will be addressed in Subsec. II-C, below.

C. *Numerical estimation of the decay from the MRS signal*

Already at the previous ICT.OPEN conference, we presented numerical estimation of the MRS decay function [5]. For the sake of simplicity, we then had to impose the restriction that the form of the decay be equal for each metabolite species in the tissue. Later on, we succeeded in lifting this restriction. To begin with, this required simulation of decay functions that depend on the metabolite species shown in Fig. 3, using the spectral domain. Each of the ten species was given its own shape. The estimation of metabolite concentrations is then done in two successive stages:

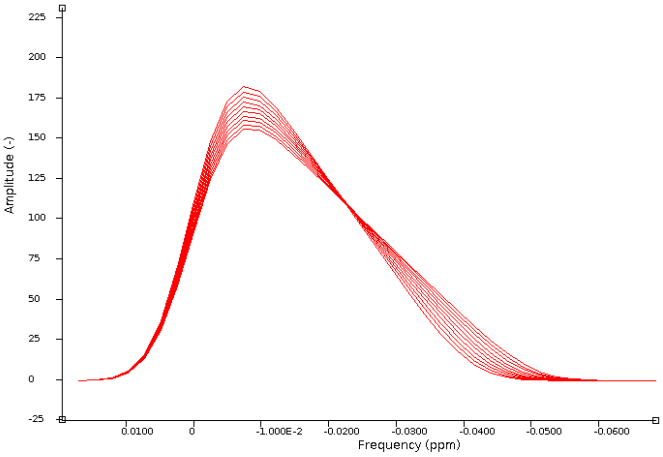

Figure 3. Real parts of the Fourier transforms of the different decays (= line-shapes) of $M = 10$ different metabolite species, FFT$[d_m(t), m = 1, 2, \ldots, M]$. In conformity with MR-custom, the polarity of the horizontal axis has been reversed and the unit is ppm of the nuclear precession frequency, here 500 MHz. The vertical axis spans the 'amplitude' of the line-shape, in arbitrary units. The asymmetry of the lineshape implies that the decay is far from the customary single exponential $e^{\alpha t}$. Figure made with the free software package jMRUI, http://www.mrui.uab.es/mrui/.

[1] This is a subject of future resarch.

[2] We adapted our description of Figure 5h in Ref. [3] to ICT.OPEN readers.

[3] Note that in MRS-context resonance and precession are synonyms.

[4] In Ref. [3] the nuclei under investigation are not metabolites but protons of mobile water in *in vivo* tissue in the human brain.

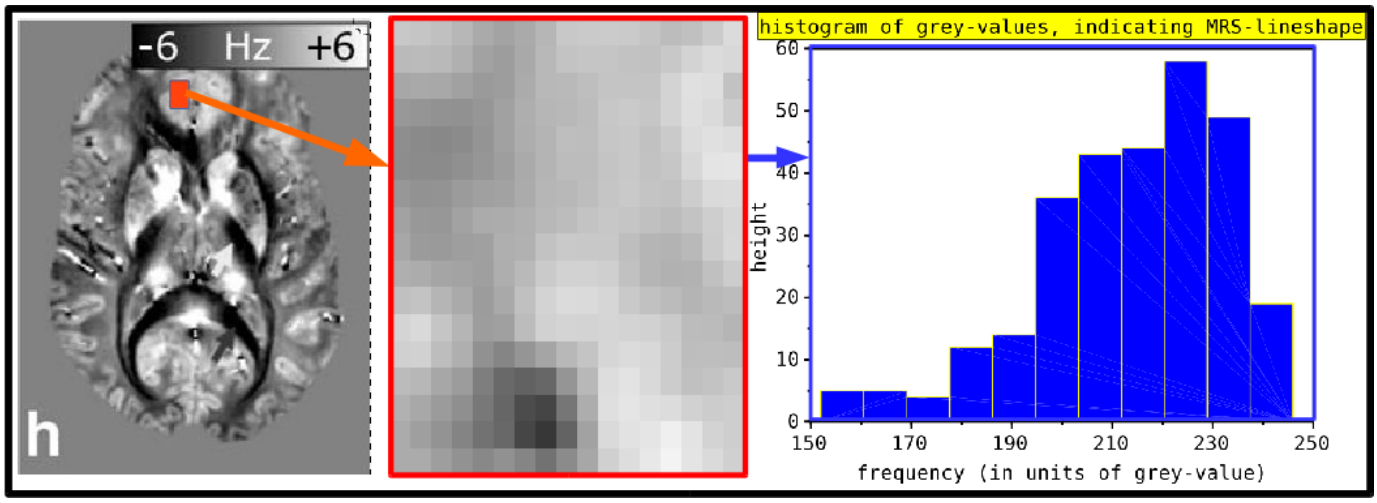

Figure 2. **Left-hand side:** A '$B_{\rm local}(\vec{r}) - B_{\rm average}$ image' of a healthy brain, Fig. 5h, taken from Ref. [3], with permission from Wiley. The field difference is shown in units of the corresponding nuclear precession (resonance) frequency difference (shift). **Middle:** The zoomed content of a small rectangle contained in the larger orange rectangle on the left. Produced with the free Gnu Image Manipulation Program GIMP. **Right-hand side:** Histogram of the grey values of the image in the middle Figure, produced with GIMP and edited with the free program Scilab. Note that the histogram is asymmetric. This happens with most rectangles selected in the frequency-shift image on left-hand side. The shape of the histogram is to be convolved with the *in vivo* MRS spectral line-shape that one would measure if the magnetic field were homogeneous. The resulting shape will still be asymmetric.

Stage 1. The model functions of the decays of all metabolite species are kept equal during the NLLS model fit, as done in Ref. [5]. The estimated concentrations $c_m, m = 1, 2, \ldots, M$, are compared to their corresponding estimated Cramér-Rao Bounds, CRB_{c_m}, $m = 1, 2, \ldots, M$. If a metabolite species, say m, has a ratio c_m/CRB_{c_m} above a certain user-supplied threshold value, its decay function is deemed eligible for improvement in stage 2, below. The decay functions of metabolite species whose ratio is found below the threshold, remain unchanged.

Stage 2. In this new approach we re-estimate the decays of eligible metabolite species on an individual basis. Eligibility pertains to SNR, *i.e.*, only high-concentration metabolite species merit further treatment. Consider a high-concentration metabolite species #m. From the model parameters estimated in stage 1, we reconstruct the measured signal, but thereby omit metabolite species #m. In other words, the reconstruction lacks the contribution from metabolite species #m itself. Subtracting this incomplete reconstruction from the measured signal, one obtains a surrogate measurement of metabolite species #m only, but including the original noise. The latter single-metabolite signal can be handled naturally with our single-decay method of Ref. [5]. The resulting estimate of $d_m(t)$ is substituted in Eq.(1). This procedure is applied consecutively for each metabolite species selected on the basis of its concentration. Finally, Eq.(1) with improved decays is fitted to the data, resulting in improved estimates of the concentrations c_m of the selected metabolite species.

III. Results

A. *Asymmetry of magnetic field inhomogeneity histograms*

From recent Quantitative Susceptibility Mapping literature [3], we produced histograms of local mesoscopic magnetic field inhomogeneity in a human head at B = 7 Tesla. Recall from Sec. II-B that the inhomogeneity of a magnetic field within a voxel of interest, $B_{\rm local}(\vec{r})$, is proportional to the shifts of the precession (resonance) frequencies of magnetic nuclei, *e.g.*, protons, at position $\vec{r}$. Fig. 2, right-hand side, shows the histogram of precession frequencies at an arbitrarily chosen location in the MRI frequency-shift map of water protons on the left-hand side. The shape of this histogram is seen to be distinctly asymmetric. The same was found for histograms derived at most other locations in the tissue. Anticipating on a worst-case scenario, we adapted our metabolite quantitation algorithm to treating each metabolite species separately, *i.e.*, with its own decay function, and this in consecutive single-species rounds, applied in stage 2, described in Sec. II-C. This is the subject of the next Subsection.

B. *Estimating decays of individual metabolite species*

As mentioned in Subsec II-C, we can now cope with the case that each metabolite species m has its own decay function, which differs from the other $M-1$ decay functions; Fig. 3 displays each. The widths of these M line-shapes change linearly, *i.e.*, not randomly, with m; this piece of information is used later on.

We tested our enhanced metabolite quantitation on noiseless and noisy simulated signals. Fig. 4 shows the results for stage 2 graphically. On the left-hand side is the noiseless case, on the right-hand side is one of the thousand different noisy cases used. The upper spectrum on either side

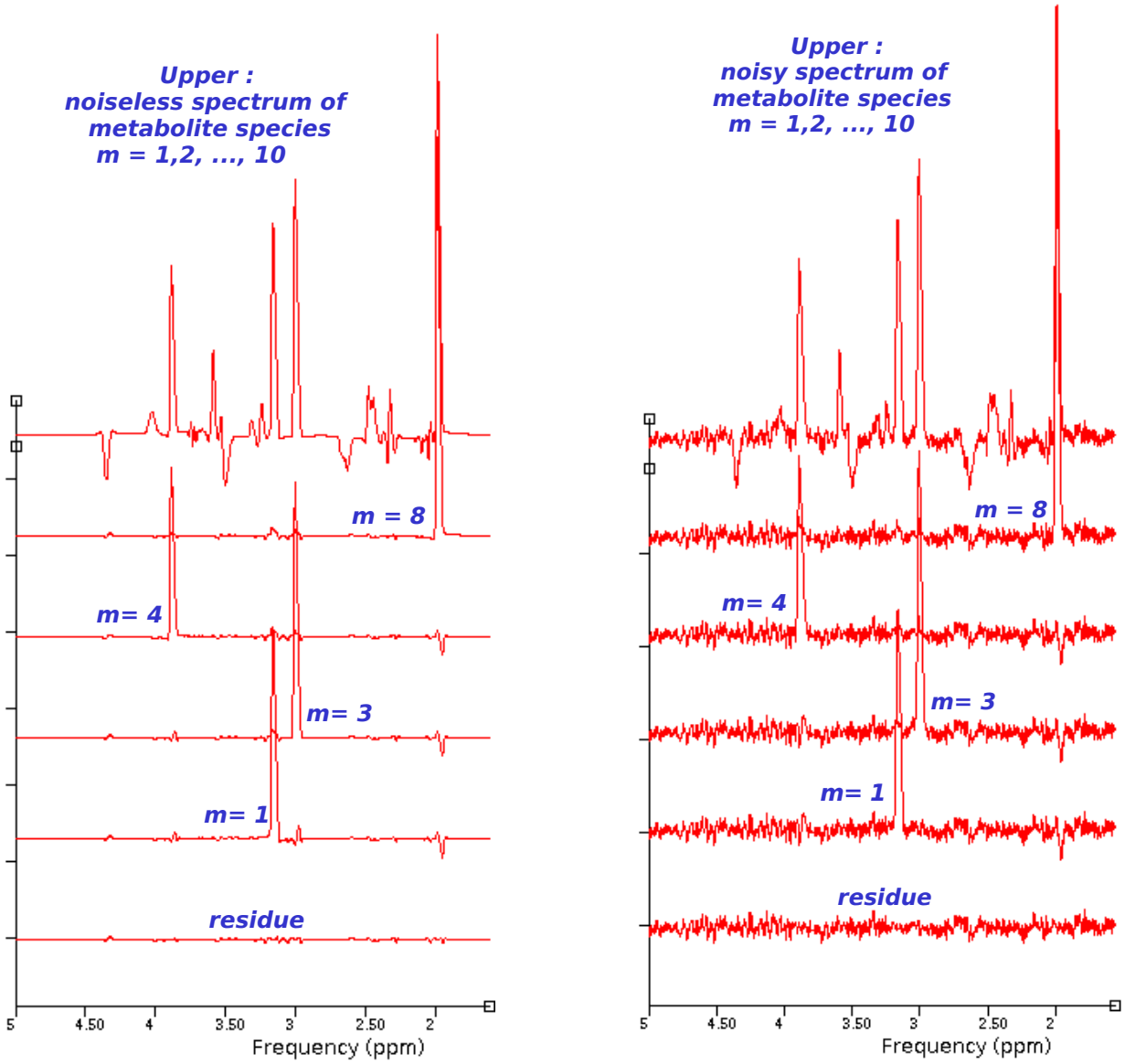

Figure 4. Illustration of estimation of metabolite concentrations for the case that the temporal decays of all metabolite species $d_m(t)$ differ from each other as indicated by FFT$[d_m(t), m = 1, 2, \ldots, M]$ in Fig. 3. Figure made with the free software package jMRUI, http://www.mrui.uab.es/mrui/.
Left: Noise is zero. Under this condition the estimation error consists only of the inherent bias of the method. The upper trace is the spectrum of the entire noiseless signal, the bottom trace is the spectrum of the residue of the model fit. In between are the spectra of separate decay functions estimated in stage 2. Only cases $m = 1, 3, 4, 8$ are shown. The other values of m were truly included in stage 2 though. See also Table I.
Right: Noise added, in a Monte Carlo simulation. The result for noise realisation #1 is shown. The setup of the Figure equals that on the left, but now stage 2 was applied only to the four metabolite species with the signal-to-noise ratio (SNR), namely $m = 1, 3, 4, 8$. The residue, at the bottom, contains mostly noise, *i.e.*, evidence of bias is not visible by eye. See also Table I.

depicts Re[FFT(signal)], whereas the bottom spectra are the residues of the estimates. The spectra in between are the estimated individual line-shapes of the four most concentrated metabolite species, namely $m = 1, 3, 4, 8$.

Noiseless Signal In the noiseless case, stage 2 was carried out for each m. This was clearly beneficial for the more concentrated metabolite species, $m = 1, 3, 4, 8$. After zooming the Figure, it can be seen that absence of noise does not result in a zero residue (bottom). The latter fact is to be expected because the application of low-pass filtering in our method is approximative [5].
Columns 2 and 3 (out of 7) in Table I show the errors in the estimated concentrations in absence of noise. The standard deviations being zero here, of course, the incurred errors equal the inherent biases of our estimator. The pattern in the signs in column 2 reflects the mentioned linear increase

Table I
ERRORS IN ESTIMATED METABOLITE CONCENTRATIONS. ¶

¶	Noiseless		With noise ⋆			
	Stage	Stage	Stage	Stage	Stage	Stage
m	1 †	2 † $	1 ‡	1 ◇	2 ‡ §	2 ◇ §
1	-0.057	0.007	0.083	-2.4	0.046	-0.37
2	-0.027	0.039	0.057	-0.3	0.059	-0.37
3	-0.031	0.010	0.064	-1.7	0.045	-0.49
4	-0.009	0.005	0.040	-0.8	0.043	-0.10
5	-0.022	-0.034	0.052	-0.4	0.055	-0.55
6	0.002	-0.008	0.091	-0.03	0.082	0.04
7	0.011	-0.025	0.020	1.1	0.019	-0.03
8	0.083	-0.004	0.062	1.2	0.062	-0.99
9	0.014	-0.013	0.027	0.3	0.026	0.13
10	0.006	0.005	0.028	0.3	0.028	-0.33

¶ Metabolite names and true concentrations corresponding to $m = 1, 2, \cdots, 10$ are listed in the **Appendix**, page 6.
⋆ Monte Carlo simulation with thousand noise realisations.
† Bias. ‡ RMSE = $\sqrt{(\text{bias}^2 + \text{stdev}^2)}$. ◇ BSR = bias/stdev.
'Stage' is introduced on page 3. $ Stage 2 done for all m.
§ Stage 2 done for $m = 1, 3, 4, 8$ only.

of the line-shape with m. As already said above, stage 2 was applied for each value of $m = 1, \ldots, M$. However, for consistency with the noisy case, Fig. 4 shows only decay estimations for the four most concentrated metabolite species.

Noisy Signal Next, we turn to the noisy case which aims to approximate the real world. At the chosen noise level, only metabolite species $m = 1, 3, 4, 8$ were judged sufficiently concentrated to qualify for improved estimation in stage 2. Thousand different noise realisations, with equal standard deviations and zero mean were used by means of a Monte Carlo simulation. In none of these, the estimation failed, indicating robustness. Fig. 4 shows the results for noise realisation #1. Table I lists the Root Mean Square Errors (RMSE's) and the bias-to-stdev ratios (BSR's) of the estimated concentrations (stdev = standard deviation). The RMSE's are in columns 4 and 6, for stages 1 and 2 respectively. The BSR's are in columns 5 and 7, for stages 1 and 2 respectively. These results are discussed in Sec. IV, below.

IV. DISCUSSION

The present manuscript addresses two aspects of importance to near-future MRS of humans at magnetic fields $\geq$ 11.7 T. As mentioned in Sec. I, these are

1) What will be the forms of the temporal decays of the MRS signals of the various metabolite species in humans at such high field strengths?
2) How to estimate concentrations of metabolite species when the forms of their temporal signal decays are unknown?

Below, we discuss our results pertaining to these issues.

A. Prediction of non-exponential temporal decay

In MRI, the study of Quantitative Susceptibility Mapping (QSM) has become an important issue [6]. A byproduct of QSM is imaging (mapping) of the shift of precession (resonance) frequencies of the protons of tissue water; see example in Fig. 2, and Sec. III-A. Some remarks are in order here.

First, the shape of an inhomogeneity histogram will depend on the locations $\vec{r}$ of the nuclei of interest in the inhomogeneous magnetic field $B_{\text{local}}(\vec{r})$. In MRS, one is primarily interested in the protons of metabolites rather than in protons of water. As remarked by Najac *et al.*, results of so-called *diffusion-weighted* MRS (DWMRS) indicate that metabolites and the bulk of water molecules reside on different locations [7]. Unfortunately, DWMRS is still in its infancy due to low signal-to-noise (SNR). Therefore, detailed information on the location of the various metabolite species in living tissue, both inter- and extra-cellular, is presently scant. As a result, the decay function of metabolites can not be predicted. Moreover, the possibility that it is different for each metabolite species can not be excluded.

Second, the histogram of Fig. 2 is based on sub-mm spatial resolution. Variations on micron-scale or nano-scale have been averaged out. However it seems likely that tissue heterogeneity on those small scales can still have appreciable effect [3]. So, even if the frequency shift displayed in Fig. 2 would be equal everywhere, an asymmetric lineshape can not be excluded.

Third, the frequency shift image is two-dimensional, whereas an MRS voxel is three-dimensinal, *e.g.*, $2 \times 2 \times 2$ cm^3. This precludes accurate estimation of an MRS lineshape from a two-dimensional frequency shift image.

B. Coping with a priori unknown temporal decay

The lack of a physical model function implies that one has to resort to semi-parametric estimation with its inherent bias. As a consequence, the handy theory of Cramér-Rao bounds (CRBs) is not applicable, implying that estimation errors can not be predicted. In Ref. [5] we presented a method to estimate the decay function from the MRS-data but with the restriction that the decay functions of all metabolite species be equal (*i.e.*, in stage 1). As a consequence of this restriction, the upper five biases in columns 2 and 5 of Table I have equal sign, whereas the sign of the lower five biases is reversed.[5] Fig. 2 and Table I, columns 3 and 7, show that lifting the restriction of equal decays (stage 2) has a significant favourable impact for the more concentrated metabolite species.

This constitutes a major result of our work.

Noiseless signal The left-hand sides of the mentioned Figure and Table pertain to the noiseless case. They indicate the sizes of the biases incurred in the estimation process. The numbers in columns 2, 3 of the Table can serve as absolute

[5] We deem the exception for $m = 6$ in column 5 insignificant because the absolute value of -0.03 is low.

lower bounds of estimation errors incurred under various circumstances. In absence of reliable CRBs, this is useful.
The nature of the biases has not yet been fully analysed. Certainly, the manner in which we apply low-pass filtering in our estimator contributes to bias [5]. Therefore, even when the unknown signal decay is equal for all metabolite species, bias is already present. Attempts to minimise this bias were so far inconclusive. As expected, biases increase further when the signal decays of the various metabolite species differ. As intended, subsequent application of stage 2 achieves reduction of the biases for the more concentrated metabolite species. Even though noise is absent, biases for the low-concentration metabolite species do not decrease in stage 2. An explanation of the latter fact may have to do with the way we apply low-pass filtering, but at present this is merely speculative.

Noisy signal The right-hand sides of Fig. 2 and Table I pertain to the noisy case. First of all, note that the residue at the bottom of the Figure seems to contain noise only. This constitutes a qualitative indication that fitting with the decays obtained in stage 2 was successful. However, a single noise realisation is insufficient for judging the performance of an estimator. Therefore we carried out a Monte Carlo simulation with as many as thousand noise realisations. The estimator performed well for all realisations.
Among other useful things, a Monte Carlo simulation yields the bias-to-stdev ratios (BSR's) listed in columns 5 and 7 of Table I. The BSR's of the high-concentration metabolite species $m = 1, 3, 4, 8$ are seen to benefit significantly. However, the BSR's for low-concentration metabolite species $m = 2, 5, 6, 7, 9, 10$ do not change significantly. Since only only high-concentration species were included in stage 2, this seems logic.
As for the RMSE's, stage 2 produced a significant effect only for $m = 1, 3$, not for $m = 4, 8$. In our opinion, this inconsistency between results for BSR's and RMSE's is circumstantial and does not imply some general trend. In this context, we mention that iteration of stage 2 with 'judiciously' distributing improved decay functions of species $m = 1, 3, 4, 8$ over species $m = 2, 5, 6, 7, 9, 10$ did not yet yield results worth mentioning here.
Finally, we point out that selecting metabolite species for treatment in stage 2 needs to be automated. A suitable selection criterion for this is sought. In any case, the program remains stable when low-concentration metabolite species are included in stage 2.

V. Concluding Remarks

1) We found evidence that lines-shapes may be asymmetric for MRS of metabolites at magnetic fields as strong as ≥ 11.7 Tesla. Moreover, the line-shapes may be different for each metabolite species.
2) We provided a stable method for quantitation of metabolite species with *a priori* unknown line-shapes.

Acknowledgements

This work was done in the context of FP7 - PEOPLE Marie Curie Initial Training Network Project PITN-GA-2012-316679-TRANSACT, http://www.transact-itn.eu/index.php, based in part on the free software package jMRUI, http://www.mrui.uab.es/mrui/.
DvO and RdB are hosted by the Imaging Physics Department, Faculty TNW, TUDelft.

References

[1] P. Vedrine and G. Gilgrass and G. Aubert and J. Belorgey and C. Berriaud and A. Bourquard and P. Bredy and A. Donati and O. Dubois and F. P. Juster and H. Lannou and F. Molinié, M. Nusbaum and F. Nunio and A. Payn and L. Quettier and T. Schild and L. Scola, and A. Sinanna, and V. Stepanov, "Iseult/INUMAC Whole Body 11.7 T MRI Magnet," IEEE TRANSACTIONS ON APPLIED SUPERCONDUCTIVITY, vol. 25, no. 3, pp. 4 301 404, 4 pp, June 2015. 1

[2] D.K. Deelchand, P-F. Van de Moortele, G. Adriany, I. Iltis, P. Andersen, J.P. Strupp, J.P. Vaughan, K. Uğurbil, and P-G. Henry, "*In vivo* ^{1}H NMR spectroscopy of the human brain at 9.4 T: Initial results," *Journal of Magnetic Resonance*, vol. 206, pp. 74–80, 2010. 1

[3] S. Wharton and R. Bowtell, "Effects of White Matter Microstructure on Phase and Susceptibility Maps," *Magnetic Resonance in Medicine*, vol. 73, pp. 1258–1269, 2015. 1, 2, 3, 5

[4] D. van Ormondt, D. Graveron-Demilly, D.M. Sima, S. Van Huffel, and S.R. Williams, *Time-Domain Methods for Quantifying MR Spectra*, ser. eMagRes. Wiley, 2015, vol. 4, ch. DOI 10.1002/9780470034590.emrstm1427, pp. 651–662. 1

[5] D. van Ormondt, R. de Beer, J.W.C. van der Veen, D.M. Sima, and D. Graveron-Demilly, "Improved estimation of the temporal decay function of in vivo metabolite signals," in *Proceedings ProRISC, ICT.OPEN 2015*. Amersfoort, The Netherlands: IPN, STW, NWO, 24-25 March 2015, pp. 36–41, http://www.ictopen2015.nl/content/Proceedings+2015. 1, 2, 3, 4, 5, 6

[6] Y.Wang and T. Liu, "Quantitative Susceptibility Mapping (QSM): Decoding MRI Data for a Tissue Magnetic Biomarker," *Magnetic Resonance in Medicine*, vol. 73, pp. 82–101, 2015. 5

[7] C. Najac, C. Marchadour, M. Guillermier, D. Houitte, V. Slavov, E. Brouillet, P. Hantraye, V. Lebon, and J. Valette, "Intracellular metabolites in the primate brain are primarily localized in long fibers rather than in cell bodies, as shown by diffusion-weighted magnetic resonance spectroscopy," *NeuroImage*, vol. 90, pp. 374–380, 2014. 5

Appendix

Table II
NAMES AND CONCENTRATIONS (AMPLITUDES) OF METABOLITE SPECIES INVOLVED IN THIS WORK. COPIED FROM REF. [5].
THE FOUR METABOLITE SPECIES WITH THE HIGHEST CONCENTRATION, c_m, ARE NUMBERED WITH RED.

m	Abbreviated	Species name	True c_m
1	Cho1	choline singlet	1.75497
2	Cho2	choline multiplet	0.19210
3	Cr1	creatine singlet 1	2.06735
4	Cr2	creatine singlet 2	1.35626
5	Glu	glutamate	0.63300
6	Gln	glutamine	0.14723
7	mI	myo-inositol	0.55275
8	NAA1	NAA singlet	2.97423
9	NAA2	NAA multiplet	0.66087
10	sI	scyllo-inositol	0.11991

2016-03-24, 11:22